Inorganic Chemistry

pubs.acs.org/IC Article

Room-Temperature Stable Ln(II) Complexes Supported by 2,6-Diadamantyl Aryloxide Ligands

Lauren M. Anderson-Sanchez, Jason M. Yu, Joseph W. Ziller, Filipp Furche,* and William J. Evans*



Cite This: Inorg. Chem. 2023, 62, 706-714

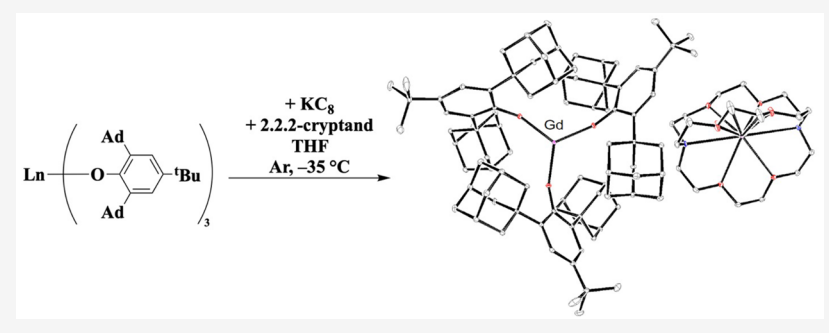


ACCESS

III Metrics & More

Article Recommendations

Supporting Information



ABSTRACT: The sterically bulky aryloxide ligand OAr^* ($OAr^* = {}^-OC_6H_2$ - Ad_2 -2,6 tBu -4; Ad = 1-adamantyl) has been used to generate Ln(II) complexes across the lanthanide series that are more thermally stable than complexes of any other ligand system reported to date for $4f'd^1$ Ln(II) ions. The Ln(III) precursors $Ln(OAr^*)_3$ (1-Ln) were synthesized by reacting 1.2 equiv of $Ln(NR_2)_3$ ($R = SiMe_3$) with 3 equiv of $HOAr^*$ for Ln = La, Ce, Nd, Gd, Dy, Yb, and Lu. 1-Ce, 1-Nd, 1-Gd, 1-Dy, and 1-Lu were identified by single-crystal X-ray diffraction studies. Reductions of 1-Ln with potassium graphite (KC_8) in tetrahydrofuran in the presence of 2.2.2-cryptand (crypt) yielded the Ln(II) complexes $[K(crypt)][Ln(OAr^*)_3]$ (2-Ln). The 2-Ln complexes for Ln = Nd, Complexes of their <math>1-Complexes of thei

INTRODUCTION

The redox landscape of the lanthanide metal (Ln) series changed upon the discovery that Ln(II) ions for all of the metals (except Pm due to its radioactivity) were available in crystallographically characterizable molecular complexes. ^{1–7} Previously, this was only possible for the six Ln(II) ions of Nd, Sm, Eu, Dy, Tm, and Yb. ^{6,7} Surprisingly, the new Ln(II) ions formed from the reduction of $4f^n$ Ln(III) precursors exhibited $4f^n$ 5d ground-state electron configurations rather than the $4f^{n+1}$ electron configurations previously observed for the original six Ln(II) ions. ^{6,7} The new Ln(II) ions were isolated in trigonal ligand environments such as $(Cp''_3Ln)^-$ and $(Cp'_3Ln)^-$ [$Cp'' = C_5H_3(SiMe_3)_2$ and $Cp' = C_5H_4(SiMe_3)_1$, where a d_2 2-like orbital was comparable in energy to the 4f0 orbitals such that a 4f'5d electron configuration was lowest in energy. ^{1–5}

Following the discovery of the $(Cp''_3Ln)^-$ and $(Cp'_3Ln)^-$ complexes, a variety of other ligand systems, such as C_5Me_4H (Cp^{tet}) , 8C_5H_4Me (Cp^{Me}) , 9C_5H_4CMe_3 (Cp^t) , ${}^{10}C_5{}^{i}Pr_5$, ${}^{11}NR_2$

(R = SiMe₃),^{12,13} and [(Ad,MeArO)₃mes],¹⁴⁻¹⁶ have been found to support 4f'5d¹ Ln(II) ions.¹⁷ Even though the coordination chemistry of the new 4f'5d¹ Ln(II) ions has been expanded, the factors affecting their successful synthesis and stability are still not clear. The results presented here explore the ability of a sterically demanding aryloxide ligand to support 4f'Sd¹ Ln(II) complexes across the lanthanide series.

More specifically, we report here that the aryloxide ligand OAr^* ($OAr^* = OC_6H_2Ad_2$ -2,6- tBu -4; Ad = 1-adamantyl)¹⁹ can support $4f'^5Sd^1$ electron configurations for Ln = La, Ce, Nd, Gd, Dy, and Lu as well as a $4f'^{t+1}$ electron configuration for Ln

Received: July 28, 2022 Published: January 3, 2023





$$1.2 \text{ Ln}(NR_2)_3 + 3 \text{ HO} \xrightarrow{-t_{Bu}} toluene, Ar, 100 °C \qquad Ln \xrightarrow{-t_{Bu}} O \xrightarrow{-t_{Bu}} 1$$

$$Ln = La, Ce, Nd, Gd, Dy, Yb$$

$$R = SiMe_3$$

$$1-Ln$$

= Yb. This ligand scaffold was previously employed to isolate the Y(II) complex [K(crypt)][Y(OAr*)₃],¹⁹ which proved to be much more stable than the analogous [K(crypt)][Y- $(OAr')_3$] (crypt = 2,2,2-cryptand; $OAr' = OC_6H_2$ - tBu_2 -2,6-Me-4) complex that had tert-butyl groups in the 2 and 6 positions rather than adamantyl groups. The Lu(II) complex [K(crypt)][Lu(OAr*)₃] was also reported in a study describing the unusually large 3467 MHz hyperfine coupling constant for the 4f145d1 Lu(II) ion and its associated clock transition.^{20,21} Although the yttrium study highlighted the importance of steric crowding for the isolation of a Y(II) ion and the lutetium study proved that this ligand scaffold could also aid in the isolation of a Lu(II) ion, it was unknown whether this ligand scaffold would allow for the isolation of Ln(II) ions of the larger lanthanide metals because these [Ln(OAr*)₃] complexes would be less sterically saturated. Additionally, it was not known whether $[Ln(OAr^*)_3]^$ complexes of the larger metals would exhibit thermal stabilities larger than those previously reported for Ln(II) complexes with large metals. This study was initiated to determine the limits in the ability of the OAr* ligand to support molecular species of Ln(II) ions.

Ad = 1-Adamantyl

RESULTS AND DISCUSSION

Syntheses and Structures of the Lanthanide(III) Aryloxide Precursors Ln^{III}(OAr*)₃ (1-Ln). The Ln(OAr*)₃ complexes (Ln = La, Ce, Nd, Gd, Dy, and Yb) were synthesized by protonolysis of 1.2 equiv of $Ln(NR_2)_3$ (R = $SiMe_3$)²² with 3 equiv of HOAr* (HOAr* = HOC₆H₂Ad₂-2,6-tBu-4) in toluene at 100 °C for 3-5 days (eq 1). An excess of the amide complex was used to minimize the presence of residual HOAr*, which has proven to be difficult to separate from the rare-earth metal product.¹⁹ The 1-Ln complexes were isolated as white powders for Ln = La, Nd, and Dy, beige powders for Ln = Ce and Gd, and red solids for Ln = Yb. The cerium complex, 1-Ce, is fluorescent (see the Experimental Section). The ¹H and ¹³C NMR spectra of La(OAr*)₃ (1-La) confirmed the presence of (OAr*)- along with trace amounts of unreacted HOAr*, as evidenced by a small peak at 5.05 ppm corresponding to the phenol hydrogen (Figures S1 and S2). The IR spectra of 1-La, 1-Nd, 1-Gd, 1-Dy, and 1-Yb also showed the presence of unreacted HOAr*, as seen by weak signals around 3600 cm⁻¹ corresponding to the characteristic O-H stretch of HOAr* (Figures S3-S8). Spectroscopic and analytical data on 1-Y¹⁹ and 1-Lu²⁰ have previously been published and establish benchmark data for this series with diamagnetic complexes. NMR spectra for these complexes and the paramagnetic complexes in this study are in the Supporting Information (SI).

Colorless crystals of **1-Gd** and **1-Dy** suitable for single-crystal X-ray diffraction studies were obtained after 1 day by dissolving the beige and white powders in boiling hexanes and cooling to room temperature (Figure 1). Different conditions were needed to isolate light-green crystals of **1-Ce** and light-

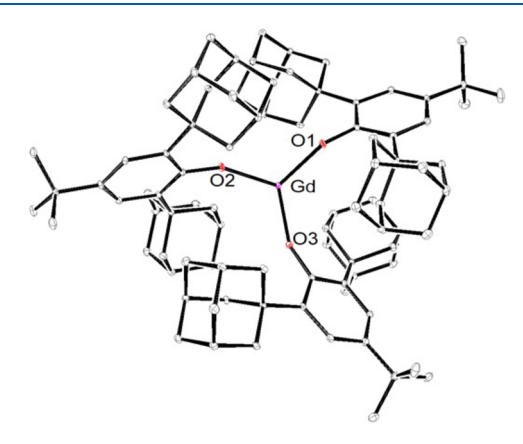


Figure 1. ORTEP representation of **1-Gd** with displacement ellipsoids drawn at the 50% probability level. For clarity, H atoms and solvent molecules are not shown.

blue crystals of 2-Nd, which were obtained after 1 week from concentrated pentane solutions at -35 °C. The crystal structure for 1-Gd is shown in Figure 1.

All of the 1-Ln complexes crystallize in the $P2_1/n$ space group and have pseudo- C_3 symmetry about the Ln metal center. The 1-Ln complexes are structurally similar but are not isomorphous because they contain different crystallization solvents in the lattice. 1-Ce and 1-Nd have 3 and 2 equiv of pentane in the lattice, respectively, whereas 1-Gd and 1-Lu have 3 and 2 equiv of hexane in the lattice, respectively. No evidence of residual HOAr* is present in the crystals. Selected metrical parameters for 1-Ln are reported in Table 1 alongside those of the previously synthesized yttrium and lutetium analogues $1-Y^{19}$ and 1-Lu. Table 1 also includes the Guzei G parameter, which is a measure of the amount of steric saturation about the central metal atom, with 100% being total saturation.

The similarity of the 1-Ln complexes is shown by the O–Ln–O and L–O– $C_{\rm exo}$ angles, which vary little from complex to complex. The average Ln–O bond lengths for 1-Y, 1-Ce, 1-Nd, 1-Gd, and 1-Lu are in agreement with each other when differences in the metal ionic radii are taken into account, ²⁴ as shown by the similarity of the average Ln–O distances adjusted for the metal ionic radius. Although the pyramidalization of the complexes shows a general trend that puts the metal atom further out of the O_3 plane for the smaller metals, it is not completely monotonic (Figure S9).

Guzei G parameters were calculated from the X-ray diffraction data to evaluate the steric saturation at the metal center. It was expected that metals with smaller ionic radii will have increased steric saturation and thus a larger G parameter. This was found to be true: **1-Ce** has the smallest G value (85%), and Lu has the largest (92%).

Syntheses and Structures of the Lanthanide(II) Aryloxide Complexes [K(crypt)][Ln^{II}(OAr*)₃] (2-Ln) and [K(18-crown-6)][Ln^{II}(OAr*)₃] (3-Ln). Solutions of 1-Ln (Ln

Table 1. Selected Bond Distances (Å) and Angles (deg) of 1-Ln^a

	1-Ce	1-Nd	1-Gd	1-Y	1-Lu
Ln-O	2.144(4)-2.151(4)	2.118(2)-2.128(2)	2.073(3)-2.111(3)	2.038(1)-2.069(1)	2.002(2)-2.020(2)
average Ln-O	2.149(2)	2.124(1)	2.089(2)	2.049(3)	2.012(1)
average $(Ln-O) - Ln(III)$ ionic radius	1.139(2)	1.140(1)	1.151(2)	1.149(3)	1.160(3)
average O-Ln-O angle	118.38(9)	118.46(4)	115.83(1)	115.69(4)	113.96(5)
average Ln-O-C _{exo}	149.2(1)	147.46(5)	150.06(5)	150.38(4)	148.16(5)
$OAr_{cent} - C_{para} - C_{exo}$ angle	173-176	172-177	177-178	177-178	177-178
$\delta(\text{Ln-O}_3\text{plane})$	0.275	0.264	0.433	0.431	0.500
G (%)	85	86	87	92	92

 $^a\delta$ is the displacement (Å) of the metal center from the O_3 plane of the three aryloxide ligands. OAr_{cent} is the centroid of the C_6 aryloxide ring. C_{para} is the carbon in the 4 position of the C_6 aryloxide ring. C_{exo} is the tertiary carbon bonded to the 4 position of the aryloxide ring. G is the Guzei G parameter and is listed as a percent. For this comparison, the six-coordinate Ln(III) ionic radii are used because this is the smallest coordination number available across the series. 24

= La, Nd, Gd, Dy, and Yb) and crypt in tetrahydrofuran (THF) react with excess potassium graphite (KC_8) at -35 °C to yield dark-blue solids of **2-Ln** for Ln = La, Nd, and Dy, a dark-purple solid for Ln = Gd, and an olive-green solid for Ln = Yb (eq 2). Reacting **1-Ce** with crypt and KC_8 at -35 °C produces a dark-blue solution that fades to colorless within 1 min; therefore, solids were not isolated from this reaction. However, a reduced cerium complex was isolated using 18-crown-6 (18-c-6; see below).

Recrystallization of these solids from diethyl ether (Et₂O) at -35 °C yielded darkly colored crystals of **2-Nd**, **2-Gd**, and **2-Dy** and bright-green crystals of **2-Yb**, identified by single-crystal X-ray diffraction studies. All four crystals are isomorphous and crystallize in the $P\overline{1}$ space group with two molecules of Et₂O in the lattice (Figure 2).

Although darkly colored solids of **2-La** could be isolated and characterized via UV—visible spectroscopy, single crystals of **2-La** suitable for crystallographic studies could not isolated. However, when the potassium chelate 18-c-6 was substituted for crypt, dark-purple crystals of $[K(18-c-6)][La(OAr^*)_3]$ (3-

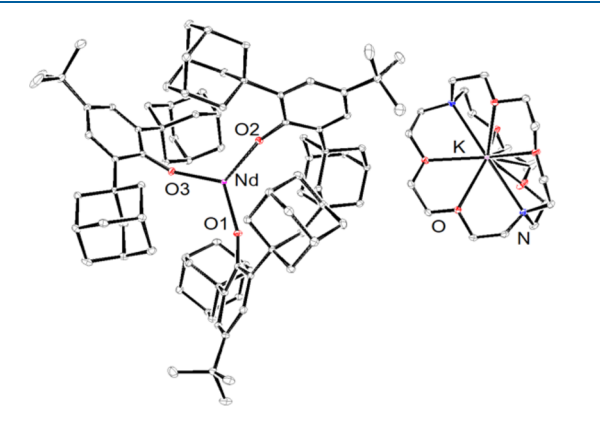


Figure 2. ORTEP representation of 2-Nd with displacement ellipsoids drawn at the 50% probability level. For clarity, H atoms and solvent molecules are not shown. The structures of 2-Y, 2-Gd, 2-Dy, 2-Yb, and 2-Lu are isomorphous.

La) were obtained and structurally characterized (eq 2 and Figure S11). Similarly, dark-purple crystals of [K(18-c-6)][Ce(OAr*)₃] (3-Ce) could be obtained and crystallographically characterized by reacting a solution of 1-Ce and 18-c-6 in Et₂O with excess KC₈ at -35 °C. Selected metrical parameters for 2-Ln and 3-Ln are reported in Table 2 alongside those of [K(crypt)][Y(OAr*)₃] (2-Y)¹⁹ and [K-(crypt)][Lu(OAr*)₃] (2-Lu).²⁰

The metrical data of the $[Ln(OAr^*)_3]^-$ anions in 2-Y, 2-Nd, 2-Gd, 2-Dy, and 2-Lu are similar to those of 3-La and 3-Ce; i.e., the nature of the countercation does not affect the structures of the Ln(II) anions. As in the 1-Ln series, the O-Ln-O and L-O-C_{exo} angles for 2-Y, 3-La, 3-Ce, 2-Nd, 2-Gd, 2-Dy, and 2-Lu vary only slightly from complex to complex. These six complexes all show increases in planarity upon reduction compared to their 1-Ln analogues. For 1-Ln, the metals were 0.254-0.500 Å out of the plane versus 0.105-0.172 Å for 2-Y, 3-La, 3-Ce, 2-Nd, 2-Gd, 2-Dy, and 2-Lu.

The changes in the Ln–O bond distances resulting from the reductions of 1-Ln to 2-Ln and 3-La are of interest because this has become a structural data point indicative of the electron configuration. Ln(II) complexes with nontraditional $4f^nSd^1$ electron configurations typically show bond elongations between 0.02 and 0.05 Å upon reduction, whereas traditional $4f^{n+1}$ electron configurations show greater bond elongations between 0.1 and 0.2 Å following the difference in the ionic radii.^{6,7} The average Ln–O bond distances for 2-Y, 3-Ce, 2-Nd, 2-Gd, 2-Dy, and 2-Lu are between 0.038 and 0.087 Å longer than those found in 1-Ln; this is consistent with nontraditional $4f^nSd^1$ electron configurations. The difference between 1-Y and 2-Y is 0.062 Å, which is appropriate for the $4d^1$ Y(II) ion.

Complex **2-Yb** is different from the other **2-Ln** complexes, however. A direct comparison of the Ln(III) and Ln(II) Ln–O bond lengths for Yb is not possible because an X-ray structure of **1-Yb** has not yet been obtained. However, the Yb–O distance in **1-Yb** can be estimated by extrapolating data from the other Ln^{III}(OAr*)₃ complexes. Using a plot of the Ln–O bond lengths as a function of the ionic radii for Ln = Y, Ce,

Table 2. Selected Bond Distances (Å) and Angles (deg) of 2-Ln and 3-Ln^a

	3-La	3-Ce	2-Nd	2-Gd	2-Dy	2-Y	2-Yb	2-Lu
Ln-O	2.2567(17) -2.2739(18)	2.228(2) -2.241(2)	2.154(2) -2.161(2)	2.154(1) -2.165(1)	2.125(1) -2.138(1)	2.106(2) -2.118(4)	2.182(1) -2.189(1)	2.062(2) -2.074(2)
average Ln-O	2.2671(9)	2.236(1)	2.157(1)	2.15867(8)	2.13077(7)	2.111(6)	2.1876(1)	2.068(3)
average $Ln-O - Ln(III)$ ionic radius	1.2351(9)	1.226(1)	1.177(1)	1.221(8)	1.219(7)	1.211(6)	1.318(1)	1.207(3)
average O-Ln-O angle	119.43(4)	119.50(4)	119.74(5)	119.75(3)	119.76(3)	119.63(6)	119.96(2)	119.50(5)
average Ln-O-C _{exo}	151.29(3)	151.16(5)	149.94(5)	149.64(3)	149.57(2)	150.50(5)	147.56(4)	150.95(5)
OAr _{cent} -C _{para} -C _{exo} angle	174-175	174-175	176-178	176-178	174-178	175-177	176-179	175-178
$\delta(\text{Ln-O}_3 \text{ plane})$	0.172	0.158	0.109	0.108	0.105	0.125	0.043	0.147
G (%)	84	84	85	86	86	90	91	91

" δ is the displacement (Å) of the metal atom from the O₃ plane of the three aryloxide ligands. OAr_{cent} is the centroid of the C₆ aryloxide ring. C_{para} is the carbon in the 4 position of the C₆ aryloxide ring. C_{exo} is the tertiary carbon bonded to the 4 position of the aryloxide ring. G is the Guzei G parameter²³ and is listed as a percent. For this comparison, the six-coordinate Ln(III) ionic radii is used because this is the smallest coordination number available across the series.²⁴

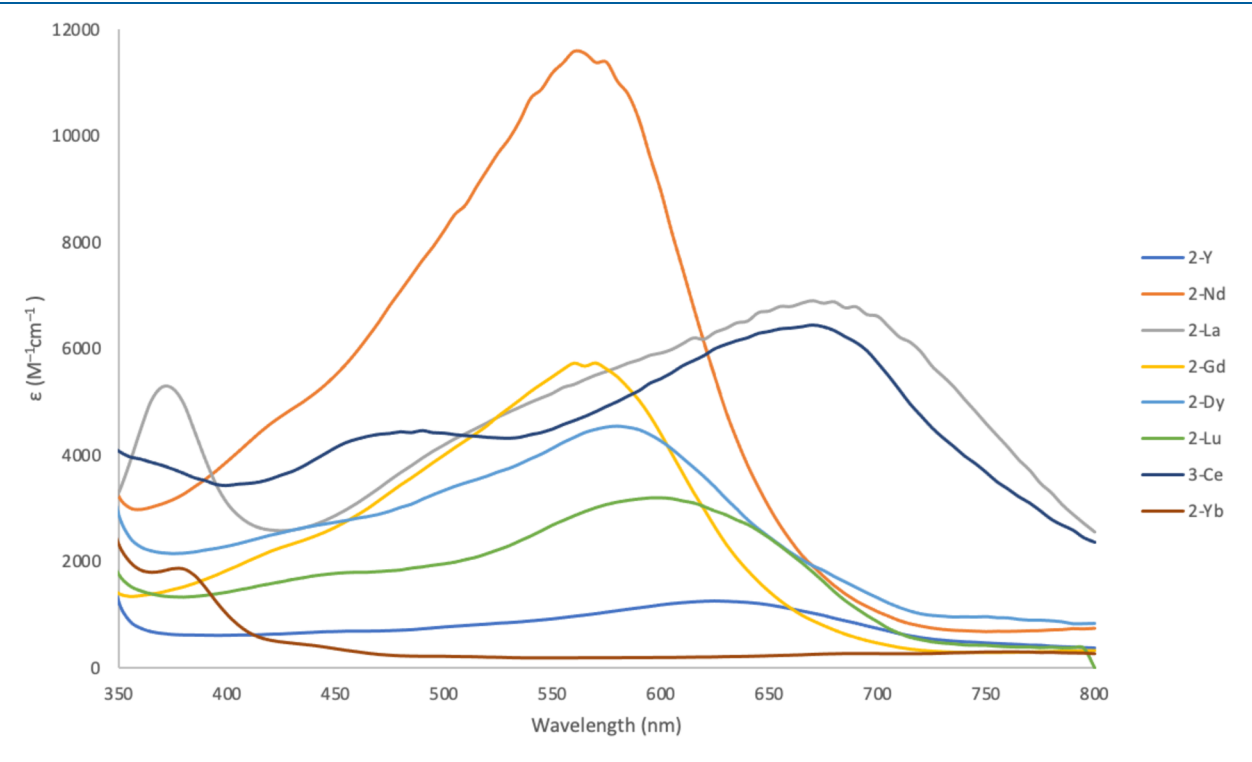


Figure 3. UV-visible spectra for 2-Ln and 3-La alongside those of 2-Y and 2-Lu.

Nd, Gd, and Lu, Figure S12, an average Yb–O bond length of 2.02 Å was estimated for 1-Yb. Using the estimated Ln–O bond length for 1-Yb, a bond elongation of 0.17 Å upon reduction was found for 2-Yb. This is consistent with a traditional $4f^{14}$ electron configuration for 2-Yb rather than a nontraditional $4f^{13}Sd^1$ electron configuration. All other divalent Yb(II) complexes also adopt traditional $4f^{14}$ electron configurations, which can be explained by the quantum-mechanical stabilization energy associated with a completely filled 4f shell. Complex 2-Yb is the most planar of all of the complexes because the Yb atom is only 0.043 Å out of the O_3 plane.

The calculated Guzei G parameters for 3-La, 3-Ce, 2-Nd, 2-Gd, and 2-Lu are only slightly smaller, by 1–2%, than their trivalent precursors, which is consistent with the slight lengthening of the Ln–O bonds. All 2-Ln and 3-Ln complexes have G parameters similar to those previously reported for the crystallographically characterized complexes $[K(\text{crypt})][Sc-(OAr')_3]$ and 2-Y. 18,19 The calculated G parameters for the

Ln(II) complexes **2-Ln** and **3-Ln** are also consistent with the hypothesis that metals with larger ionic radii will have lower calculated G parameters, similar to what was observed for the Ln(III) precursors **1-Ln**. The large size of the OAr^* ligand clearly allows steric saturation across the lanthanide series.

UV–Visible Spectroscopy. Figure 3 shows the absorbance spectra for **2-Ln** and **3-Ln** alongside those of the previously reported complexes **2-Y**¹⁹ and **2-Lu**. Complexes **2-Nd**, **2-Gd**, and **2-Dy** show strong absorbances around 565 mm with calculated molar attenuation coefficients, ε , of 7000, 4500, and 6300 M⁻¹ cm⁻¹, respectively. These λ_{max} and ε values are similar to those of **2-Y** and **2-Lu** reported earlier. Complex **2-La** has a strong absorbance at 670 nm (ε = 9000 M⁻¹ cm⁻¹) as well as an additional absorbance at 372 nm (ε = 5300 M⁻¹ cm⁻¹). **3-Ce** also exhibits a strong absorbance at 670 (ε = 6600 M⁻¹ cm⁻¹) as well as an additional, smaller absorbance at 490 nm (ε = 4500 M⁻¹ cm⁻¹). In contrast, **2-Yb** shows weak absorbances at 375, 510, 685, and 755 nm, with calculated molar attenuation coefficients of 1500, 200, 200, and

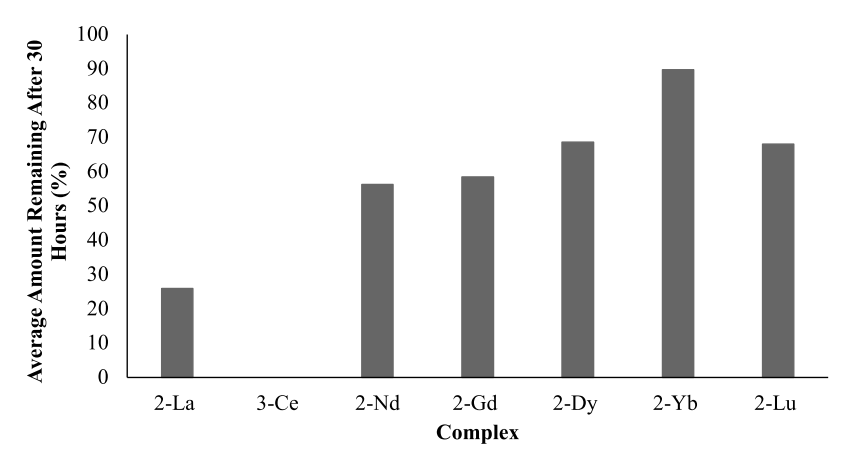


Figure 4. Percent remaining of the Ln(II) complexes 2-Ln and 3-Ce after 30 h. The reported values are averages calculated over three separate runs.

300 M⁻¹ cm⁻¹, respectively. The lower molar attenuation coefficient of **2-Yb** versus the other **2-Ln** complexes is also characteristic of the 4fⁿ⁺¹ versus 4fⁿ5d¹ electron configurations. ⁵⁻⁷

Thermal Decomposition Studies. The thermal stabilities of 2-Ln and 3-Ln at room temperature were assessed using UV—visible spectroscopy. Previously, it was shown that 2-Y is stable for 48 h at room temperature, whereas the Y(II) complex synthesized with the 2,6-di-tert-butyl aryloxide complex, [K(crypt)][Y(OAr')₃], decomposed in 60 s. ¹⁹ Absorption spectra of freshly prepared samples of 2-La, 3-Ce, 2-Nd, 2-Gd, 2-Dy, 2-Yb, and 2-Lu in THF at room temperature were taken every 1 h for 30 h to evaluate the thermal stabilities. These kinetic studies were performed in triplicate, and Figure 4 reports the average percent remaining of each Ln(II) complex after 30 h. The detailed data are given in Figures S41—S52.

In contrast to the stabilities of the Ln(II) complexes 2-Ln (Ln = La, Nd, Gd, Dy, Yb, and Lu), 3-Ce proved to be the least stable complex in this series, with none remaining after 30 h (Figure 4). Decomposition of 3-Ce was then monitored over a shorter period of time, 8.5 h, by taking absorption spectra every 15 min (Figure S44). After 8.5 h, 23% of 3-Ce was present. Figure 4 also shows that the 4f¹⁴ Yb(II) complex, 2-Yb, is the most stable of the other Ln(II) complexes in this series, because 94% of 2-Yb is still present after 30 h at room temperature. This is consistent with the fact that the 4f¹⁴ Yb(II) ion is a much weaker reductant than the 4f¹⁵Sd¹ Ln(II) ions in this study; this has been observed in other series of Ln(II) complexes.^{5-7,35} Overall, these 2-Ln complexes are the most stable complexes ever isolated for these 4f⁶Sd¹ Ln(II) ions.

These results, alongside the calculated solid G values, highlight the important role that the 2,6-substituents of the phenol ring play in providing steric saturation at the metal center. The previously examined aryloxide ligand OAr', which contains *tert*-butyl groups at the 2 and 6 positions, only provided sufficient steric saturation for the smallest rare-earth metal, Sc, to be isolated in the 2+ oxidation state as $[K(\text{crypt})][Sc(\text{OAr'})_3]$; this Sc(II) complex had a calculated G parameter of 83%. The analogous Ln(II) complex for the larger metal Y decomposed within a minute and had a low estimated calculated G parameter of 77%. In contrast, the isolated Ln(II) complexes with adamantyl groups at the 2 and 6 positions, i.e., 2-Ln (Ln = Y, Nd, Gd, Dy, Yb, and Lu) and 3-

La, have *G* parameters ranging from 84% to 91% and decompose very slowly at room temperature. These results provide evidence to support the idea that steric factors play an important role in the successful isolation of Ln(II) complexes. However, the instability of 3-Ce indicates that steric factors alone are inadequate to explain all of the observed data.

Electronic Structure Calculations. Density functional theory (DFT) was used to elucidate the ground-state electronic structures and excited-state properties of the [Ln(OAr*)₃]⁻ anions in 2-Ln for Ln = La, Nd, Gd, Dy, Yb, and Lu. The TPSSh functional²⁵ was used for all compounds, and the resolution-of-the-identity (RI) approximation²⁶ was used to speed up integral computations. The def2-TXVP basis sets²⁷ were used for each Ln metal center, and the def2-SVP basis sets were used for ligand atoms. A small-core effective core potential with scalar-relativistic corrections²⁸ was used to describe the core electrons. In addition, D3 dispersion corrections²⁹ and the implicit solvation model COSMO³⁰ were used for each calculation. Experimental structures in the form of crystallographic data were used as the starting points.

The population analysis results are consistent with the predicted electronic configurations of $4f''5d^1$ for **2-Ln**, where Ln = La, Gd, Dy, and Lu (Table S1). On the other hand, for [Nd(OAr*)₃]⁻ (**2-Nd**), the highest occupied molecular orbital (HOMO) exhibited a mixture of 4f, 5d, and 6s character, suggesting the presence of low-lying excited states and multiconfigurational character for this species. This behavior has been observed previously in DFT studies of [Nd- $(C_5H_4SiMe_3)_3$]⁻ complexes⁵ and is consistent with Nd(II) being a configurational crossover ion that can access both $4f^3Sd^1$ and $4f^4$ electron configurations. 5-7 Calculations on [Yb(OAr*)₃]⁻ were consistent with a $4f^{14}$ electron configuration and a doubly occupied HOMO.

The calculated Ln–O bond distances (Table 3) parallel the experimental values, which decrease across the series for Ln = La, Nd, Gd, Dy, and Lu due to the lanthanide contraction. Both the calculations and experimental data are consistent with small increases in the bond distances for $4f^{15}d^{1}$ Ln(II) ions compared to their $4f^{1}$ Ln(III) analogues and larger increases for $4f^{1+1}$ Ln(II) ions like $4f^{14}$ Yb(II) compared to $4f^{13}$ Yb(III). The calculated values for the $4f^{0}5d^{1}$ La(II) and $4f^{14}5d^{1}$ Lu(II) ions are closest to the experimental values, which may be related to their empty and filled 4f shells.

Time-dependent DFT studies predict optical spectra for the $[Ln(OAr^*)_3]^-$ anions that also match the experimental data

Table 3. Averaged Calculated versus Experimental Ln-O Bond Distances for the $[Ln(OAr^*)_3]^-$ Anions with Calculated Geometries Optimized Using Scalar-Relativistic DFT

Ln-O bond	calcd (Å)	exptl (Å)		
La-O	2.30	2.28		
Nd-O	2.25	2.16(3)		
Gd-O	2.20	2.16(2)		
Dy-O	2.20	2.13(1)		
Lu-O	2.07	2.07(3)		
Yb-O	2.17	2.19(3)		

quite well. Calculations for $4f^{n}Sd^{1}$ Nd(II), Gd(II), Dy(II), and Lu(II) ions predict a single major envelope of absorptions, and the calculation for La(II) indicates two absorption bands (Figure 5). This is exactly what is observed experimentally (Figure 3). In addition, the prediction for the $4f^{14}$ Yb(II) complex indicates absorptions of much lower intensity, as observed experimentally. Calculations on $[Ce(OAr^*)_3]^-$ gave an electronic structure that was numerically unstable, and it was not possible to get an excited-state spectrum for this system. The cerium system differed from the other compounds in that $Ce(OAr^*)_3$ (1-Ce) is fluorescent and its reduction product requires 18-c-6 rather than crypt chelation in order to isolate a solid.

CONCLUSION

The 2,6-diadamantyl-substituted aryloxide ligand $OC_6H_2Ad_2$ -2,6- tBu -4 (OAr^*) has provided the most stable series of $4f''5d^1Ln(II)$ complexes isolated to date. The stability of the $[Ln(OAr^*)_3]^-$ complexes originally observed for $Ln=Y^{19}$ carries over to the other metals in the series, with the surprising exception of Ln=Ce. The stability of the $4f''5d^1La(II)$, Nd(II), Gd(II), Dy(II), and Lu(II) complexes demonstrates the importance of steric saturation for Ln(II) ions, as is already well-known for Ln(III) compounds. However, the less stable cerium example points out that steric

factors alone are not enough to fully describe the stability of complexes of the $4f^n5d^1$ Ln(II) ions. This series also reinforces the differences between complexes of Ln(II) ions with $4f^n5d^1$ and $4f^{m+1}$ electron configurations because the $4f^{14}$ Yb complex exhibits longer Ln–O bond distances, a less intense optical spectrum, and greater stability than the $4f^n5d^1$ complexes.

■ EXPERIMENTAL SECTION

All manipulations and syntheses described below were conducted with the rigorous exclusion of air and water using standard Schlenkline and glovebox techniques under an argon atmosphere. Solvents were sparged with ultrahigh-purity argon and dried by passage through columns containing Q-5 and molecular sieves prior to use. Deuterated NMR solvents were dried over NaK alloy, degassed by three freeze-pump-thaw cycles, and vacuum-transferred before use. ¹H and ¹³C NMR spectra were recorded on CRYO500 MHz or ADVANCE600 MHz spectrometers at 298 K unless otherwise stated and referenced internally to residual protio-solvent resonances. UVvisible spectra were collected in THF at room temperature in a 0.1 cm Schlenk cuvette fitted with a Teflon stopcock using an Agilent Cary 60 UV-visible spectrometer. IR transmittance measurements were taken as compressed solids on an Agilent Cary 630 Fourier transform infrared spectrophotometer with a diamond ATR attachment. Fluorescence intensity measurements were performed on an Agilent Cary Eclipse fluorescence spectrometer at room temperature using a 1 cm quartz cuvette. The excitation and emission slit widths were set at 5 and 2.5 nm, respectively. Elemental analytical data were collected on a Thermo Scientific FlashSmart CHNS/O elemental analyzer. As was previously found for 2-Y¹⁹ and 2-Lu,²⁰ obtaining good analytical data on this class of complexes has been problematic.^{38–41} 2.2.2-Cryptand (VWR) was dried under reduced pressure (10⁻³ Torr) before use. ⁻⁴¹ 2.2.2-Cryptand $HOAr^*$, 32,33 $Ln(NR_2)_3$ (R = $SiMe_3$)²² and KC_8 ³⁴ were synthesized using published preparations. Caution!KC8is a known pyrophoric reagent and appropriate precautions should be taken when handling this material.

 $La(OAr^*)_3$ (1-La). In an argon-containing glovebox, $La[N-(SiMe_3)_2]_3$ (300 mg, 0.484 mmol) and HOAr* (507 mg, 1.21 mmol) were combined in toluene (40 mL) in a 100 mL Schlenk flask containing a Teflon-coated stir bar and fitted with a Teflon stopcock. The sealed clear light-yellow solution was stirred and heated to 100 $^{\circ}C$ in an oil bath. After 5 days, the solution was cooled to room

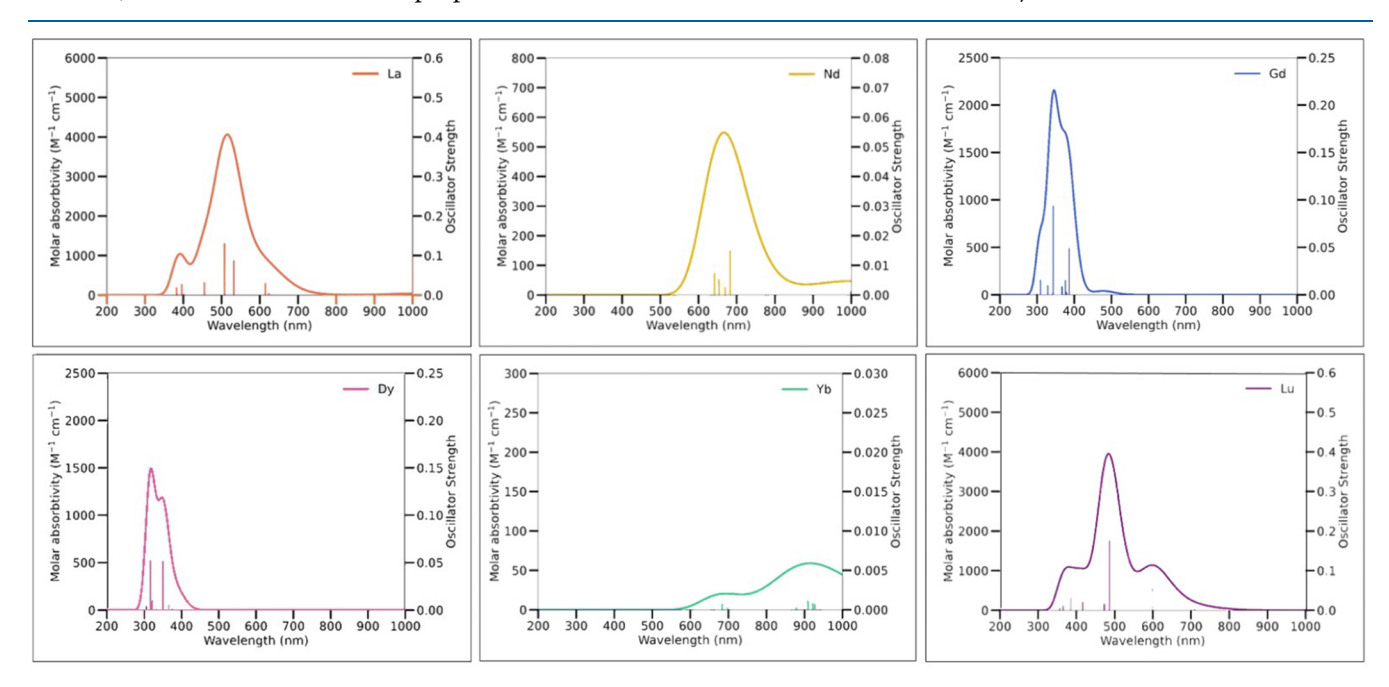


Figure 5. Simulated UV-visible spectra for Ln(II) complexes 3-La, 2-Nd, 2-Gd, 2-Dy, 2-Yb, and 2-Lu.

temperature and the solvent was removed under vacuum to yield light-yellow oily solids. The oily solids were dissolved in 20 mL of hexanes and transferred to a 25 mL scintillation vial, where the solvent was removed again in vacuo to yield beige oily solids. These solids were washed three times with 4 mL of pentane and dried under vacuo to yield 1-La as a powdery white solid (343 mg, 61%). ¹H NMR (C_6D_6) : δ 7.32 (s, 6H, m-H), 5.06 (s, 1H, O-H), 3.58 (s, residual methanol), 2.44 (d, J = 11.6 Hz, 18H, Ad-CH₂, proximal to the C₆ ring), 2.30 (d, J = 11.6 Hz, 18H, Ad-CH₂, proximal to the C₆ ring), 2.06 (s, 18H, Ad-CH), 1.74 (d, J = 11.9 Hz, 18H, Ad-CH₂ distal to the C₆ ring, overlapping with the corresponding resonance in $HOAr^*$), 1.69 (d, J = 11.61 Hz, 18H, Ad-CH₂ distal to the C₆ ring, overlapping with the corresponding resonance in HOAr*), 1.44 (s, 27H, t-Bu, overlapping with the corresponding resonance in HOAr*). ¹³C NMR (C_6D_6) : δ 159.20 (*i*-C), 138.70 (*o*-C), 135.20 (*p*-C), 128.00 (residual HOAr*), 127.80 (residual HOAr*), 127.70 (residual HOAr*), 127.50 (residual HOAr*), 121.50 (m-C), 43.70 (Ad-CH₂, proximal to the C₆ ring), 37.90 (quaternary C, from Ad or t-Bu), 37.20 (Ad-CH₂, distal to the C₆ ring), 34.50 (quaternary C, from Ad or t-Bu), 31.90 (CMe₃), 29.40 (Ad-CH). IR (cm⁻¹): 3630w br, 2937m sh, 2898s, 2842s, 2652w, 1586w, 1474m sh, 1442s, 1422s, 1349w sh, 1362m, 1344m, 1292m, 1254m, 1239s, 1202m sh, 1178w, 1116w, 1105m, 1047w, 988w, 975m, 949w, 883w sh, 841m, 833s, 820m sh, 811m sh, 772m, 755m, 723s, 693w, 662w.

 $Ce(OAr^*)_3$ (1-Ce). $Ce[N(SiMe_3)_2]_3$ (156 mg, 0.251 mmol) was reacted with HOAr* (254 mg, 0.607 mmol), as described above for 1-La, for 5 days to yield an olive-green solution. The solvent was removed under vacuum to yield oily olive-green solids. Crystals of 1-Ce suitable for X-ray crystallography were grown over 2 weeks by dissolving the oily olive-green solids in pentane and placing them in a-35 °C freezer. Complex 1-Ce exhibits fluorescence, as shown in the Figure S10 spectrum. Fluorescence: $\lambda_{\rm ex}$ = 427 nm, $\lambda_{\rm em}$ = 544 nm. UV-vis [room temperature, THF; λ , nm (ε , M⁻¹ cm⁻¹)]: 427 (4000). ¹H NMR (C_6D_6): δ 11.49, 7.39, 5.09, 3.18, 2.63, 2.21, 2.12, 2.03, 1.73, 1.41, 1.25, 0.89, 0.10, -0.82, -1.63, -2.67, -4.52. ¹³C NMR (C_6D_6): δ 156.20, 146.27, 135.36, 121.53, 43.63, 41.28, 40.33, 37.65, 36.98, 36.58, 34.21, 32.72, 31.74, 31.60, 29.23, 25.34, 22.70, 22.39, 14.00, 13.93. IR (cm⁻¹): 3632w br, 2937m sh, 2899s, 2848s, 2654w, 1746w, 1597w, 1437m sh, 1424s, 1388w, 1360m, 1342m, 1310w, 1256m, 1236m sh, 1226s, 1198s sh, 1135m, 1098m, 1077w, 1023w, 975m, 921w, 872m, 833s, 809s, 766m, 727s, 693w, 662w.

 $Nd(OAr^*)_3$ (1-Nd). $Nd[N(SiMe_3)_2]_3$ (200 mg, 0.320 mmol) was reacted with HOAr* (335 mg, 0.800 mmol), as described above for 1-La, for 2 days to yield a light-turquoise solution. The solvent was removed under vacuum to yield oily turquoise solids, which were then dissolved in 20 mL of hexanes, transferred to a 25 mL scintillation vial, and redried to yield oily turquoise solids. The resulting solids were dissolved in 25 mL of pentane and cooled to −35 °C to yield light-blue crystals of 1-Nd (179 mg, 48%). 1 H NMR ($C_{6}D_{6}$): δ 17.11, 7.22, 6.97, 5.25, 4.22, 2.29, 2.19, 2.10, 1.81, 1.48, 1.33, 0.95, 0.17, -5.04, -5.95, -8.12, -9.89. ¹³C NMR (C_6D_6): δ 184.73, 157.76, 152.20, 141.59, 135.36, 133.02, 128.93, 125.43, 121.53, 49.12, 41.31, 38.11, 37.99, 37.64, 36.99, 34.58, 34.10, 31.73, 29.23, 22.71, 22.37, 20.94, 20.64, 13.91, 2.26. IR (cm⁻¹): 3630w br, 2939m sh, 2898s, 2846s, 2652w, 1586w, 1469m, 1444s, 1424s, 1390w, 1359m, 1342m, 1290m, 1277s, 1243s, 1202m sh, 1176m, 1161m sh, 1101m, 1090w sh, 1055w sh, 1047w, 1019w sh, 978m, 948w, 939w sh, 921w sh, 883w, 876m, 831s, 820s sh, 808m sh, 779w sh, 772m, 757w, 727s, 693w, 660w.

Gd(OAr*)₃ (1-**Gd)**. Gd[N(SiMe₃)₂]₃ (150 mg, 0.235 mmol) was reacted with HOAr* (246 mg, 0.588 mmol), as described above for 1-La, to yield 1-Gd as a white powder (175 mg, 63%). Crystals suitable for X-ray crystallography were grown by slow heating of a solution of 1-Gd in hexanes until fully dissolved and then allowing the solution to cool to room temperature overnight. ¹H NMR (C_5D_5N): δ 8.77, 7.59, 7.41, 7.23, 3.71, 2.29, 1.67, 1.27, 0.91. ¹³C NMR (C_5D_5N): δ 67.78, 47.52, 31.55, 25.71, 22.79, 14.22. IR (cm⁻¹): 3632w br, 2894s, 2842s, 2652w, 1746w, 1597w, 1440m sh, 1423s, 1390w, 1359m, 1288m, 1293m, 1275s, 1240s sh, 1227s, 1200s sh, 1103m, 1098m, 1046w, 977m, 921m, 872m, 839s, 807s sh, 770m, 725m, 663w, 659w.

Dy(OAr*)₃ (1-**Dy).** Dy[N(SiMe₃)₂]₃ (151 mg, 0.235 mmol) was reacted with HOAr* (244 mg, 0.583 mmol), as described above for 1-La, to yield 1-Dy as a white powder (144 mg, 52%). Crystals suitable for X-ray crystallography were grown over 2 weeks by slow heating of a solution of 1-Dy in hexanes until fully dissolved and then cooling in a -35 °C freezer. ¹H NMR (C_6D_6): δ 14.70, 9.11, 7.63, 7.01, 5.52, 4.16, 3.99, 3.71, 3.26, 3.09, 2.86, 1.99, -12.47, -14.07, -15.77. ¹³C NMR (C_5D_5N): δ 67.58, 41.48, 37.48, 37.03, 31.71, 29.37, 25.60, 22.65, 22.32, 13.99. IR (cm⁻¹): 3632w br, 2939m sh, 2898s, 2842s, 2792m sh, 2654w, 1748w, 1599w, 1446m sh, 1428s, 1388w, 1360m, 1344m, 1295m, 1252s, 1249s, 1243s sh, 1232s, 1198m, 1137m, 1103m, 1070w, 1034w, 977m, 919w, 827m, 844s, 811m, 768m, 732m, 695w, 659w.

Yb(OAr*)₃ (1-**Yb)**. Yb[N(SiMe₃)₂]₃ (153 mg, 0.234 mmol) was reacted with HOAr* (241 mg, 0.576 mmol), as described above for 1-La, to yield 1-**Yb** as red solids (210 mg, 77%). ¹H NMR (C_6D_6): δ 9.82, 9.59, 7.52, 5.72, 4.66, 4.47, 4.17, 3.84, 3.69, 3.33, -9.03. ¹³C NMR (C_6D_6): δ 152.50, 141.79, 135.36, 121.53, 41.30, 36.97, 34.54, 31.72, 29.22, 22.68, 13.96. IR (cm⁻¹): 3634w br, 2898s, 2846s, 2656w, 1597w, 1439s, 1428s, 1390w, 1359m, 1342m, 1293m, 1254s, 1223m sh, 1232s, 1204m sh, 1170m, 1137m, 1097m, 1040w sh, 977m, 878w, 854m, 844m, 809m sh, 764m, 725s, 665w, 662w. Elem anal. Calcd for $C_{90}H_{123}O_3$ Yb: C, 75.81; H, 8.69. Found: C, 74.55; H, 10.23

Lu(OAr*)₃ (1-Lu).²⁰ Lu[N(SiMe₃)₂]₃ (304 mg, 0.463 mmol) was reacted with HOAr* (481 mg, 1.15 mmol), as described above for 1-La, for 5 days to yield a clear yellow solution. The solvent was removed under vacuum to yield oily yellow solids, which were then redissolved in hexanes, transferred to a 25 mL scintillation vial, and then redried under vacuo to yield oily beige solids. These solids were dissolved in pentane and placed in a -35 °C freezer to yield colorless crystals of 1-Lu after 1 week.

[K(crypt)][Nd(OAr*)₃] (2-Nd). In an argon-containing glovebox, a clear light-blue solution of 1-Nd (25 mg, 0.017 mmol) and crypt (7 mg, 0.02 mmol) was prepared in THF (2 mL) and chilled to -35 °C for 1 h. The solution of 1-Nd and crypt was pipetted into a scintillation vial containing excess KC₈ (6 mg, 0.05 mmol) chilled to -35 °C and swirled to yield a dark-blue solution. The dark-blue solution was filtered through a Kimwipe-packed glass pipet to remove black solids (presumably graphite and excess KC₈). The solids were washed with chilled THF (5 mL), and the resulting filtrate was dried in vacuo to yield dark-blue solids. The dark-blue solids were triturated with hexane $(2 \times 2 \text{ mL})$ and pentane $(2 \times 2 \text{ mL})$ and redried in vacuo to yield a dark-blue solid of 2-Nd (26 mg, 81%). Crystals suitable for X-ray crystallography were grown overnight by dissolving 2-Nd in Et₂O and cooling to -35 °C. IR (cm⁻¹): 2891s, 2839s, 1477w sh, 1441m sh, 1422s, 1384w, 1354m, 1337w, 1274m sh, 1261m, 1239s, 1203w, 1170w, 1132s, 1096s, 1075s, 1028w sh, 979m, 948s, 931s, 864m, 831s, 817m, 804s, 768s, 752m, 727s, 692w, 659m. UV-vis [room temperature, THF; λ , nm (ε , M⁻¹ cm⁻¹)]: 610 (7000)

[K(crypt)][Gd(OAr*)₃] (2-Gd). A clear colorless solution of 1-Gd (25 mg, 0.018 mmol) and crypt (7 mg, 0.02 mmol) was reacted with excess KC₈ (6 mg, 0.05 mmol), as described above for 2-Nd, to yield 2-Gd as a dark-purple solid (25 mg, 76%). Crystals suitable for X-ray crystallography were grown overnight by dissolving 2-Gd in Et₂O and cooling to -35 °C. IR (cm⁻¹): 2888m, 2839m, 1474w, 1441w sh, 1425m, 1387w, 1355w, 1337w sh, 1274m, 1258m, 1240m, 1198w, 1173w, 1129m, 1099s, 1069s, 976m, 949m, 932m, 864w, 831m, 820m, 809m, 771m, 749w, 727m, 708w, 691w, 661w. UV—vis [room temperature, THF; λ , nm (ε , M⁻¹ cm⁻¹)]: 570 (4500).

[K(crypt)][Dy(OAr*)₃] (2-Dy). A clear colorless solution of 1-Dy (25 mg, 0.018 mmol) and crypt (7 mg, 0.02 mmol) was reacted with excess KC₈ (8 mg, 0.06 mmol), as described above for 2-Nd, to yield 2-Dy as a dark-blue solid (29 mg, 90%). Crystals suitable for X-ray crystallography were grown over 1 week by dissolving 2-Dy in Et₂O and cooling to -35 °C. IR (cm⁻¹): 2888m, 2839m, 1474m, 1444m sh, 1422m, 1389w, 1355m, 1337w sh, 1272m, 1258m, 1240s, 1200w, 1170w, 1127s, 1096s, 1072s, 1003w, 976m, 949s, 932m, 899w sh, 867w, 834m, 820m, 809m, 771m, 746w, 730m, 708w, 694w, 661w.

UV—vis [room temperature, THF; λ , nm (ε , M⁻¹ cm⁻¹)]: 575 (6300).

[K(crypt)][Yb(OAr*)₃] (2-Yb). A clear burnt-orange solution of 1-Yb (25 mg, 0.018 mmol) and crypt (9 mg, 0.02 mmol) was reacted with excess KC₈ (7 mg, 0.05 mmol), as described above for 2-Nd, to yield 2-Yb as a lime-green solid (26 mg, 81%). Crystals suitable for X-ray crystallography were grown overnight by dissolving 2-Yb in Et₂O and cooling to -35 °C. ¹H NMR (C₅D₅N): δ 7.41, 7.22, 3.63, 3.36, 2.73, 2.59, 2.45, 2.34, 2.17, 1.91, 1.64, 1.48, 1.30, 0.94, 0.16. ¹³C NMR (C₅D₅N): δ 88.62, 71.16, 70.45, 70.15, 67.57, 56.79, 53.79, 42.60, 41.37, 38.19, 37.42, 32.59, 32.12, 30.00, 29.59, 25.53. IR (cm⁻¹): 2956w sh, 2874m, 2842m, 1591w, 1473w, 1428m, 1388w, 1349m, 1344w, 1289m, 1256m sh, 1240m, 1201w, 1173w, 1129m, 1099s, 1063s, 1025m sh, 975m, 949m, 928m, 906m, 865m, 831s, 813s, 805m sh, 774m, 752m, 724m, 656w. UV—vis [room temperature, THF; λ, nm (ε, M⁻¹ cm⁻¹)]: 375 (1500), 510 (200), 685 (200), 755 (300).

 $[K(18-c-6)][La(OAr^*)_3]$ (3-La). In an argon-containing glovebox, a clear solution of 1-La (25 mg, 0.018 mmol) and 18-c-6 (5 mg, 0.02 mmol) was prepared in THF (2 mL) and chilled to -35 °C for 1 h. The solution of 1-La and 18-c-6 was pipetted into a scintillation vial containing excess KC₈ (5 mg, 0.04 mmol) chilled to -35 °C and swirled to yield a dark-blue solution. The dark-blue solution was filtered through a Kimwipe-packed glass pipet to remove black solids (presumably graphite and excess KC₈). The solids were washed with chilled THF (5 mL), and the resulting filtrate was dried in vacuo to yield dark-blue solids of 3-La (31 mg, 95%). Crystals suitable for Xray crystallography were grown over 1 week by dissolving the darkblue solids in Et₂O and cooling to -35 °C. IR (cm⁻¹): 2889m, 2842m, 1592w, 1474w, 1441w, 1422m, 1386w, 1353m, 1310w sh, 1272m, 1258m, 1236s, 1195w sh, 1170w, 1132s, 1099s, 1075s, 973m, 948m, 932m, 869w, 830m, 804m, 768m, 752w, 725m, 694w, 658w. UV-vis [room temperature, THF; λ , nm (ε , M⁻¹ cm⁻¹)]: 372 (5300), 665 (9000).

[K(18-c-6)][Ce(OAr*)₃ (3-Ce). In an argon-containing glovebox, a yellow solution of 1-Ce (25 mg, 0.018 mmol) and 18-c-6 (5 mg, 0.02 mmol) was prepared in Et₂O (2 mL) and chilled to -35 °C for 1 h. The solution of 1-Ce and 18-c-6 was pipetted into a scintillation vial containing excess KC₈ (5 mg, 0.04 mmol) chilled to -35 °C and swirled to yield a dark-blue solution. The dark-blue solution was filtered through a Kimwipe-packed glass pipet to remove black solids (presumably graphite and excess KC₈). The solids were washed with chilled Et₂O (5 mL), and the resulting filtrate was placed in a freezer at -35 °C, where crystals suitable for X-ray crystallography were grown overnight. UV–vis [room temperature, Et₂O; λ , nm (ε , M⁻¹ cm⁻¹)]: 490 (4500), 670 (6600).

ASSOCIATED CONTENT

Solution Supporting Information

The Supporting Information is available free of charge at https://pubs.acs.org/doi/10.1021/acs.inorgchem.2c02167.

Characterization data, NMR and IR spectra, thermal decomposition data, and crystallographic data (PDF)

Accession Codes

CCDC 2180609–2180618 contain the supplementary crystallographic data for this paper. These data can be obtained free of charge via www.ccdc.cam.ac.uk/data_request/cif, or by emailing data_request/cif, or by contacting The Cambridge Crystallographic Data Centre, 12 Union Road, Cambridge CB2 1EZ, UK; fax: +44 1223 336033.

AUTHOR INFORMATION

Corresponding Authors

William J. Evans — Department of Chemistry, University of California, Irvine, Irvine, California 92617, United States; orcid.org/0000-0002-0651-418X; Email: wevans@uci.edu

Filipp Furche — Department of Chemistry, University of California, Irvine, Irvine, California 92617, United States; orcid.org/0000-0001-8520-3971; Email: filipp.furche@uci.edu

Authors

Lauren M. Anderson-Sanchez – Department of Chemistry, University of California, Irvine, Irvine, California 92617, United States; Occid.org/0000-0002-9697-8008

Jason M. Yu — Department of Chemistry, University of California, Irvine, Irvine, California 92617, United States; orcid.org/0000-0002-2270-6798

Joseph W. Ziller – Department of Chemistry, University of California, Irvine, Irvine, California 92617, United States; orcid.org/0000-0001-7404-950X

Complete contact information is available at: https://pubs.acs.org/10.1021/acs.inorgchem.2c02167

Notes

The authors declare the following competing financial interest(s): Principal Investigator Filipp Furche has an equity interest in TURBOMOLE GmbH. The terms of this arrangement have been reviewed and approved by the University of California, Irvine, in accordance with its conflict of interest policies.

ACKNOWLEDGMENTS

We thank the U.S. National Science Foundation for support of this research under Grants CHE-2154255 (to W.J.E.) and CHE-2102568 (to F.F.) and Tyler Kerr for assistance with single-crystal X-ray diffraction. This paper is dedicated to Professor Peter C. Junk on the occasion of his 60th birthday.

REFERENCES

- (1) Hitchcock, P. B.; Lappert, M. F.; Maron, L.; Protchenko, A. V. Lanthanum Does Form Stable Molecular Compounds in the + 2 Oxidation State. *Angew. Chem., Int. Ed.* **2008**, *47*, 1488–1491.
- (2) MacDonald, M. R.; Ziller, J. W.; Evans, W. J. Synthesis of a Crystalline Molecular Complex of Y^{2+} , [(18-crown-6)K]-[(C_3H_4 SiMe₃)₃Y]. J. Am. Chem. Soc. **2011**, 133, 15914–15917.
- (3) MacDonald, M. R.; Bates, J. E.; Fieser, M. E.; Ziller, J. W.; Furche, F.; Evans, W. J. Expanding Rare-Earth Oxidation State Chemistry to Molecular Complexes of Holmium(II) and Erbium(II). *J. Am. Chem. Soc.* **2012**, *134* (20), 8420–8423.
- (4) MacDonald, M. R.; Bates, J. E.; Ziller, J. W.; Furche, F.; Evans, W. J. Completing the Series of + 2 Ions for the Lanthanide Elements: Synthesis of Molecular Complexes of Pr²⁺, Gd²⁺, Tb²⁺, and Lu²⁺. *J. Am. Chem. Soc.* **2013**, *135* (26), 9857–9868.
- (5) Fieser, M. E.; MacDonald, M. R.; Krull, B. T.; Bates, J. E.; Ziller, J. W.; Furche, F.; Evans, W. J. Structural, Spectroscopic, and Theoretical Comparison of Traditional vs Recently Discovered Ln^{2+} Ions in the $[K(2.2.2\text{-cryptand})][(C_5H_4SiMe_3)_3Ln]$ Complexes: The Variable Nature of Dy^{2+} and Nd^{2+} . J. Am. Chem. Soc. **2015**, 137, 369–382.
- (6) Woen, D. J.; Evans, W. J. Expanding the +2 Oxidation State to the Rare-Earth Metals, Uranium, and Thorium in Molecular Complexes. *Handbook on the Physics and Chemistry of Rare Earths including Actinides*; Elsevier North Holland: Amsterdam, The Netherlands, 2016; Vol. 50, pp 336–394; DOI: 10.1016/bs.hpcre.2016.08.002.
- (7) Evans, W. J. Tutorial on the Role of Cyclopentadienyl Ligands in the Discovery of Molecular Complexes of the Rare-Earth and Actinide Metals in New Oxidation States. *Organometallics.* **2016**, *35*, 3088–3100.

- (8) Jenkins, T. F.; Woen, D. H.; Mohanam, L. N.; Ziller, J. W.; Furche, F.; Evans, W. J. Tetramethylcyclopentadienyl Ligands Allow Isolation of Ln(II) Ions Across the Lanthanide Series in $[K(2.2.2-crypand)][(C_5Me_4H)_3Ln]$ Complexes. *Organometallics.* **2018**, 37, 3863–3873.
- (9) Huh, D. N.; Ziller, J. W.; Evans, W. J. Isolation of reactive Ln(II) complexes with C_5H_4Me ligands (Cp^{Me}) using inverse sandwich countercations: synthesis and structure of [(18-crown-6)K(μ -Cp^{Me})-K(18-crown-6)][Cp^{Me} $_3$ Ln^{II}] (Ln = Tb, Ho). Dalton Trans. **2018**, 47, 17285–17290.
- (10) Angadol, M. A.; Woen, D. H.; Windorff, C. J.; Ziller, J. W.; Evans, W. J. *tert*-Butyl(cyclopentadienyl) Ligands Will Stabilize Nontraditional + 2 Rare-Earth Metal Ions. *Organometallics.* **2019**, 38, 1151–1158.
- (11) Gould, C. A.; McClain, R.; Yu, J. M.; Groshens, T. J.; Furche, F.; Harvey, B. G.; Long, J. R. Synthesis and Magnetism of Neutral, Linear Metallocene Complexes of Terbium(II) and Dysprosium(II). *J. Am. Chem. Soc.* **2019**, *141* (33), 12967–12973.
- (12) Ryan, A. J.; Darago, L. E.; Balasubramani, S. G.; Chen, G. P.; Ziller, J. W.; Furche, F.; Long, J. R.; Evans, W. J. Synthesis, Structure, and Magnetism of Tris(amide) {Ln[N(SiMe₃)₂]₃}¹⁻ Complexes of the Non-Traditional + 2 Lanthanide Ions. *Chem.Eur. J.* **2018**, 24, 7702–7709.
- (13) Ryan, A. J.; Ziller, J. W.; Evans, W. J. The Importance of the Counter-cation in Reductive Rare-Earth Metal Chemistry: 18-Crown-6 Instead of 2,2,2-Cryptand Allows Isolation of [Y^{II}(NR₂)₃]¹⁻ and Ynediolate and Enediolate Complexes from CO Reactions. *Chem. Sci.* **2020**, *11*, 2006–2014.
- (14) Fieser, M. E.; Palumbo, C. T.; La Pierre, H. S.; Halter, D. P.; Voora, V. K.; Ziller, J. W.; Furche, F.; Meyer, K.; Evans, W. J. Comparisons of Lanthanide/Actinide + 2 Ions in a Tris(aryloxide)-arene Coordination Environment. *Chem. Sci.* **2017**, *8*, 7424–7433.
- (15) Palumbo, C. T.; Halter, D. P.; Voora, V. K.; Chen, G. P.; Chan, A. K.; Fieser, M. E.; Ziller, J. W.; Hieringer, W.; Furche, F.; Meyer, K.; Evans, W. J. Metal versus Ligand Reduction in Ln³⁺ Complexes of a Mesitylene-Anchored Tris(Aryloxide) Ligand. *Inorg. Chem.* **2018**, *57*, 2823–2833.
- (16) Palumbo, C. T.; Halter, D. P.; Voora, V. K.; Chen, G. P.; Ziller, J. W.; Gembicky, M.; Rheingold, A. L.; Furche, F.; Meyer, K.; Evans, W. J. Using Diamagnetic Yttrium and Lanthanum Complexes to Explore Ligand Reduction and C-H Bond Activation in a Tris-(aryloxide)mesitylene Ligand System. *Inorg. Chem.* **2018**, *57*, 12876—12884
- (17) Kelly, R. P.; Maron, L.; Scopelliti, R.; Mazzanti, M. Reduction of a Cerium(III) Siloxide Complex to Afford a Quadruple-Decker Arene-Bridged Cerium(II) Sandwich. *Angew. Chem.* **2017**, *129*, 15869–15872.
- (18) Moehring, S. A.; Beltrán-Leiva, M. J.; Páez-Hernández, D.; Arratia-Pérez, R.; Ziller, J. W.; Evans, W. J. Rare-Earth Metal(II) Aryloxides: Structure, Synthesis, and EPR Spectroscopy of $[K(2.2.2-cryptand)][Sc(OC_6H_2^tBu_2-2,6-Me-4)_3]$. Chem. Eur. J. 2018, 24, 18059-18067.
- (19) Moehring, S. A.; Miehlich, M.; Hoerger, C. J.; Meyer, K.; Ziller, J. W.; Evans, W. J. A Room-Temperature Stable Y(II) Aryloxide: Using Steric Saturation to Kinetically Stabilize Y(II) Complexes. *Inorg. Chem.* **2020**, *59* (5), 3207–3214.
- (20) Kundu, K.; White, J. R. K.; Moehring, S. A.; Yu, J. M.; Ziller, J. W.; Furche, F.; Evans, W. J.; Hill, S. A 9.2-GHz Clock Transition in a Lu(II) Molecular Spin Qubit Arising from a 3,467-MHz Hyperfine Interaction. *Nat. Chem.* **2022**, *14*, 392–397.
- (21) Wedal, J. C.; Evans, W. J. A Rare-Earth Metal Retrospective to Stimulate All Fields. J. Am. Chem. Soc. 2021, 143, 18354–18367.
- (22) Bradley, D. C.; Ghotra, J. S.; Hart, F. A. Three-co-ordination in Lanthanide Chemistry: Tris[bis(trimethylsilyl)amido]lanthanide(III) Compounds. *Chem. Soc., Chem. Commun.* 1972, 349–350.
- (23) Guzei, L. A.; Wendt, M. An Improved Method for the Computation of Ligand Steric Effects Based on Solid Angles. *Dalton Trans.* **2006**, 3991–3999.

- (24) Shannon, R. D. Revised Effective Ionic Radii and Systematic Studies of Interatomic Distances in Halides and Chalcogenides. *Acta. Crystallogr., Sect. A: Cryst. Phys., Diffr., Theor. Gen. Crystallogr.* **1976**, 32, 751–767.
- (25) Staroverov, V. N.; Scuseria, G. E.; Tao, J.; Perdew, J. P. Comparative assessment of a new nonempirical density functional: Molecules and hydrogen-bonded complexes. *J. Chem. Phys.* **2003**, *119*, 12129–12137.
- (26) Eichkorn, K.; Treutler, O.; Öhm, H.; Häser, M.; Ahlrichs, R. Auxiliary Basis Sets to Approximate Coulomb Potentials. *Chem. Phys. Lett.* **1995**, 240, 283–290.
- (27) Cao, X.; Dolg, M.; Stoll, H. Valence basis sets for relativistic energy-consistent small-core actinide pseudopotentials. *J. Chem. Phys.* **2003**, *118*, 487–496.
- (28) Cao, X.; Dolg, M. Segmented contraction scheme for smallcore actinide pseudopotential basis sets. *J. Mol. Struct.: THEOCHEM* **2004**, 673, 203–209.
- (29) Grimme, S.; Antony, J.; Ehrlich, S.; Krieg, H. A consistent and accurate ab initio parametrization of density functional dispersion correction (DFT-D) for the 94 elements H-Pu. *J. Chem. Phys.* **2010**, 132, 154104.
- (30) Klamt, A.; Schüürmann, G. COSMO: a new approach to dielectric screening in solvents with explicit expressions for the screening energy and its gradient. *J. Chem. Soc., Perkin Trans.* 2 **1993**, 2, 799–805.
- (31) Mulliken, R. S. Electronic Population Analysis on LCAO-MO Molecular Wave Functions. I. J. Chem. Phys. 1955, 23, 1833.
- (32) Watanabe, T.; Ishida, Y.; Matsuo, T.; Kawaguchi, H. Synthesis and Structures of Zirconium(IV) Complexes Supported by 2,6-diadamantylaryloxide Ligands and Formation of Arene-bridged Dizirconium Complexes with an Inverse Sandwich Structure. *Dalton Trans.* **2010**, *39*, 484–491.
- (33) Hoerger, C. J.; La Pierre, H. S.; Maron, L.; Scheurer, A.; Heinemann, F. W.; Meyer, K. Reductive Disproportionation of Nitric Oxide Mediated by Low-valent Uranium. *Chem. Commun.* **2016**, *52*, 10854–10857.
- (34) Bergbreiter, D. E.; Killough, J. M. Reactions of Potassium-Graphite. *J. Am. Soc.* **1978**, *100* (7), 2126–2134.
- (35) Trinh, M. T.; Wedal, J. C.; Evans, W. J. Evaluating electrochemical accessibility of $4f^nSd^1$ and $4f^{n+1}$ Ln(II) ions in $(C_5H_4SiMe_3)_3$ Ln and $(C_5Me_4H)_3$ Ln Complexes. *Dalton Trans.* **2021**, 50, 14384–14389.
- (36) Moehring, S. A.; Beltrán-Leiva, M. J.; Páez-Hernández, D.; Arratia-Pérez, R.; Ziller, J. W.; Evans, W. J. Rare-Earth Metal(II) Aryloxides: Structure, Synthesis, and EPR spectroscopy of [K(2.2.2-cryptand)][Sc(OC₆H₂^tBu₂-2,6-Me-4)₃]. *Chem. A. Eur. J.* **2018**, 24, 18059–18067.
- (37) Huh, D. N.; Roy, S.; Ziller, J. W.; Furche, F.; Evans, W. J. Isolation of a Square-Planar Th(III) Complex: Synthesis and Structure of $[Th(OC_6H_2^tBu_2-2,6-Me-4)_4]^{1-}$. *J. Am. Chem. Soc.* **2019**, *141*, 12458–12463.
- (38) Goodwin, C. A. P.; Chilton, N. F.; Vettese, G. F.; Moreno Pineda, E.; Crowe, I. F.; Ziller, J. W.; Winpenny, R. E. P.; Evans, W. J.; Mills, D. P. Physicochemical Properties of Near-Linear Lanthanide-(II) Bis(silylamide) Complexes (Ln = Sm, Eu, Tm, Yb). *Inorg. Chem.* **2016**, *55*, 10057–10067.
- (39) Hitchcock, P. B.; Lappert, M. F.; Maron, L.; Protchenko, A. V. Lanthanum does Form Stable Molecular Compounds in the + 2 Oxidation State. *Angew. Chem., Int. Ed.* **2008**, *47*, 1488–1491.
- (40) Goodwin, C. A.; Reta, D.; Ortu, F.; Chilton, N. F.; Mills, D. P. Synthesis and Electronic Structures of Heavy Lanthanide Metallocenium Cations. *J. Am. Chem. Soc.* **2017**, *139*, 18714–18724.
- (41) Gabbai, F. P.; Chirik, P. J.; Fogg, D. E.; Meyer, K.; Mindiola, D. J.; Schafer, L. L.; You, S. An Editorial About Elemental Analysis. *Organometallics* **2016**, *35*, 3255–3256.